Indian J Phys
https://doi.org/10.1007/s12648-024-03406-x

ORIGINAL PAPER

Search for new physics with reactor neutrino at Kuo-Sheng neutrino laboratory

S Karmakar[1,2]*, M K Singh[1]*, S Karadağ[1,3], H T Wong[1], H B Li[1], V Sharma[4], C Greeshma[1,5], M K Singh[2], L Singh[5], F K Lin[1] and V Singh[5]

[1]Institute of Physics, Academia Sinica, Taipei 115201, Taiwan

[2]Department of Physics, Institute of Applied Sciences & Humanities, GLA University, Mathura 281406, India

[3]Department of Physics Engineering, Istanbul Technical University, 34467 Istanbul, Turkey

[4]Department of Physics, H.N.B. Garhwal University, Srinagar 246174, India

[5]Department of Physics,School of Physical and Chemical Sciences, Central University of South Bihar, Gaya 824236, India

Received: 11 October 2023 / Accepted: 28 August 2024

Abstract: The observation of coherent elastic neutrino nucleus scattering by the COHERENT collaboration alongside a positive hint from the DRESDEN−II experiment propelled the study of neutrino physics beyond the Standard Model. In the current work we have explored the light mediator models scenario, along with the neutrino non-standard interactions. Apart from a very good sensitivity to study these physics scenarios, reactor neutrinos provide the benefit of working in the fully coherent region due to their abundant low energy flux. The analyzed data set in the present work comprised of 124.2(70.3) kg day reactor ON(OFF) exposure collected at Kuo-Sheng neutrino laboratory with high purity *n*-type point Germanium detector. To assess the potential influence of the quenching factor on the limits obtained, we varied the parameter k in the Lindhard model within three scenarios: conservative (0.157), intermediate (0.200), and optimistic (0.260). These choices encompass a range of currently favored values. In the absence of any discernible excess at low energy in the measured spectrum for the considered physics scenarios, we have established competitive limits with the contemporary experiments specifically focused to search for coherent elastic neutrino nucleus scattering.

Keywords: Reactor neutrino; Coherent elastic neutrino nucleus scattering; Non standard interaction; Beyond the standard model

1. Introduction

Coherent elastic neutrino-nucleus scattering (CEνNS) is a neutral current process induced by an exchange of the Z boson in which low-energy neutrinos scatter off the entire nucleus [1]. In this phenomenon, all nucleons can contribute coherently to the process since the initial and final states of the target nucleus are indistinguishable during this process [2]. Consequently, the cross section of this interaction increases tremendously ($\propto N^2$, N represents the number of neutron present in the target nucleus) and has the largest value among the other low-energy interaction channels of neutrino [3]. This interaction is limited for nucleus having dimension comparable to the inverse of momentum transfer [4].

CEνNS has remained an undiscovered phenomenon due to the lower nuclear recoil produced by neutrinos. The COHERENT collaboration has recently discovered this phenomenon (after $>$ 40 years of its prediction) with pion-decay-at-rest (π-DAR) neutrino source from the Spallation Neutron Source (SNS) at the Oak Ridge National Laboratory using CsI[Na] scintillator with 6.7σ significance [3] and liquid Argon detector with 3σ significance [5].

The neutrino fluxes in nuclear power reactors are very high, making them an appealing electron antineutrino ($\bar{\nu_e}$, hereinafter reactor neutrino) source to look for CEνNS. Recently, the Dresden-II collaboration has hinted at the possibility of detecting CEνNS with reactor neutrinos [6].

*Corresponding author, E-mail: skarmakar@gate.sinica.edu.tw; manu@gate.sinica.edu.tw

Published online: 12 September 2024

It stimulates reactor-based experiments, such as TEXONO [7], CONNIE [8], CONUS [9, 10], *v*GEN [11], RED-100 [12], CHOOZ [13], to detect CE*v*NS with full coherency (>95%) [14], which is partial for π-DAR experiments.

COHERENT experiment faces three components of neutrinos ($\nu_\mu, \nu_e, \bar{\nu}_\mu$), produced from SNS facility, where ν_μ component is produced immediately after pion decay ($\pi^+ \rightarrow \mu^+ + \nu_\mu$) with a monochromatic spectrum at 29.8 MeV, whereas the other two delayed components are generated by subsequent muon decay ($\mu^+ \rightarrow e^+ + \nu_e + \bar{\nu}_\mu$), which have a continuous spectrum with an endpoint energy of 52.8 MeV that produces nuclear recoil of $\mathcal{O}(10)$ keV [5]. Meanwhile, in reactor-based experiments, typically, four isotopes (^{235}U, ^{238}U, ^{239}Pu, and ^{241}Pu) are responsible for creating 84% of neutrinos ($\bar{\nu}_e$) from β-decay, while rest of the 16% are produced by neutron capture of ^{238}U nuclei resulting in a continuous spectrum up to 8 MeV, which generates nuclear recoil of $\mathcal{O}(1)$ keV [8, 15]. Therefore, due to the relatively low recoil energy and comparatively large backgrounds, detection of CE*v*NS with reactor neutrinos is challenging and requires a more precise understanding of sub-keV physics.

As a result of the first CE*v*NS observation (experimental evidence for the consistency of the SM), numerous fascinating searches have been triggered from conventional SM to exotic neutrino physics beyond the standard model (BSM) (see Refs. [4, 10] and references therein for more details). Together with the knowledge of expected SM interactions, any new interaction can help us in getting valuable information about the evolution of stellar collapses [16, 17], stellar nucleosynthesis [18], supernovae [19–21], etc., in cosmology [22] as well as in nuclear and particle physics [23, 24], for instance, neutron density distribution of a target nucleus [25–27], weak mixing angle in the unexplored MeV regime [28–31]. Meanwhile, observing the CE*v*NS has significant implications on neutrino floor [32–37] (an irreducible background) for Dark Matter (DM) direct detection, which is caused by atmospheric, solar, and supernova remnant neutrinos that coherently scatter in these detectors [38, 39]. CE*v*NS experiments can be used as part of BSM searches [14, 40, 41] to detect non-standard neutrino-quark interactions (NSIs) [42–49], electromagnetic properties of neutrinos [50–54] (e.g. finite magnetic moments or millicharges), investigations of light mediators (e.g. light scalars and/or axion-like particles [49, 55–57], light vectors [4, 58–60] such as dark photons), sterile neutrinos [61], neutrino generalized interactions (NGI) [62], dark large mixing angle (DLMA), and many others.

The TEXONO experiment investigates the detection of CE*v*NS using reactor neutrinos [7]. An *n*-type point-contact high purity germanium (*n*PCGe) detector was used to acquire the underlying data at a 28 m distance from the center of the reactor core (with 30 m-water-equivalent overburden) of a 2.9 GW (thermal power) nuclear plant located in New Taipei, Taiwan [15, 63–65]. The low energy threshold of *n*PCGe detectors [66, 67] make them ideal devices for searching CE*v*NS because they allow detection of low-energy nuclear recoil. Our current work focuses on investigating light mediators (scalar and vector) and NSIs (vectorial and tensorial) in the measurements of CE*v*NS with reactor neutrinos as new physics candidates BSM.

2. CE*v*NS signal expectation in the SM and beyond

CE*v*NS occurs when a neutrino of any flavor scatters off a nucleus at low momentum transfer such that the scattering amplitudes of the nucleon wave functions are in phase and can add coherently. The SM weak interaction differential cross section of CE*v*NS for a spin-zero nucleus neglecting radiative corrections, as a function of nuclear recoil energy T is given by [1]

$$\frac{d\sigma_{\rm SM}}{dT}(T, E_\nu) = \frac{G_F^2 M_N}{4\pi}\left(1 - \frac{M_N T}{2E_\nu^2}\right) Q_{\rm SM}^2 F^2(q^2)\ , \tag{1}$$

where G_F is the Fermi coupling constant, M_N is the mass of the target nuclei (e.g. Germanium as in our analysis), E_ν is the incident neutrino energy. The SM weak nuclear charge $Q_{\rm SM}$ can be expressed as

$$Q_{\rm SM} = g_p^V Z + g_n^V N \tag{2}$$

where N and Z are the neutron and proton number, respectively. The neutrino-proton and neutrino-neutron couplings are represented by symbols g_p^V and g_n^V, respectively, and can be expanded as

$$g_p^V = \frac{1}{2} - 2\,\sin^2\theta_{\rm W},\quad g_{\rm n}^{\rm V} = -\frac{1}{2},\ \text{therefore} \tag{3}$$

$$Q_{\rm SM}^2 \equiv \left[N - (1 - 4\,\sin^2\theta_{\rm W})Z\right]^2, \tag{4}$$

where θ_W is the weak mixing angle or Weinberg angle. In order to avoid complexity, we removed the factor $\left(\frac{1}{2}\right)$ from the SM weak charge expression (Eq. 4) and added an additional prefactor of $\left(\frac{1}{4}\right)$ to Eq. (1). The current analysis adopts the value of $\sin^2\theta_{\rm W}$, which is 0.23857 [59, 68] at low energies. It can be seen from the structure of the $Q_{\rm SM}$ in Eq. (4) that the nature of SM CE*v*NS is N^2 dependent due to the small prefactor associated with Z.

The nuclear form factor $F(q^2)$ is related to the physical size of the nucleus and the nuclear density distribution. In our earlier work [14, 41], we studied the effect of $F(q^2)$ at

the cross section (Eq. 1) and found a marginal effect for neutrinos with $E_\nu < 10$ MeV. Because of the low momentum transfer in CEνNS with reactor neutrinos [69], the cross section (Eq. 1) is not sensitive to the particular choice of common form factors (e.g. Helm [70], Fermi [71], Klein and Nystrand [72], etc.). It is important to note that, however, $F(q^2)$ will play a crucial role in the COHERENT experiment because of the loss of coherency for the high energy neutrinos from the π-DAR sources [14, 41]. Typically, Helm [70] or Klein and Nystrand [72] form factor parametrization describe this loss of coherent enhancement. Despite $F(q^2)$ nominal effect for reactor neutrinos, we have considered Helm parametrization [70] for $F(q^2)$ to ensure precision and completeness.

The CEνNS cross section is modified by the presence of new mediators coupled to SM neutrinos and quarks, and thus considered as an extension to the SM. COHERENT data have recently been used to explore these highly motivated models [4, 23, 40, 42–49, 73]. As mentioned in Sect. 1, two simplified extensions of the SM with light mediators [74] and NSIs are considered in the current work and they are briefly illustrated in the following subsections.

2.1. Low mass mediator

2.1.1. Light vector mediator

In the frameworks of BSM, new Z-like vector bosons ($Z^{'}$) arise in simple U(1)$^{'}$ extensions of the SM, and have been studied in various scenarios [10, 40, 75, 76]. The existence of this new mediator field could explain existing B-meson anomalies in the LHCb experiment [77] as well as solution to the DLMA [78, 79]. Although such extensions of SM have primarily been applied to DM searches, they may also be accessible to future as well as current neutrino experiments. This work focuses exclusively on the relevant parts of this extension that might contribute to CEνNS.

We first investigates potential interactions via a new $Z^{'}$ vector mediator with mass $M_{Z'}$. The interaction of a $Z^{'}$ with the left-handed neutrinos and quarks can be described by the generic Lagrangian [40]

$$\mathcal{L}_{Z'} = Z'_{\mu}\left(g_{Z'}^{qV}\bar{q}\gamma^{\mu}q + g_{Z'}^{\nu V}\bar{\nu}_L\gamma^{\mu}\nu_L\right) + \frac{1}{2}M_{Z'}^2 Z'_{\mu}Z'^{\mu}. \tag{5}$$

where $g_{Z'}^{qV}$ and $g_{Z'}^{\nu V}$ are the vector-quark and vector-neutrino coupling constants, respectively. We omit intrinsic traits such as kinetic or mass mixing and disregard interactions pertaining to the right-handed neutrino, aiming to constrain the anticipated vector and axial vector annulment. In this framework, the resultant change for BSM is presented as a scaling transformation of the SM CEνNS cross section [69, 80, 81]

$$\frac{d\sigma_{\mathrm{SM}+Z'}}{dT} = \mathcal{Q}_{Z'}^2(T)\frac{d\sigma_{\mathrm{SM}}}{dT}, \tag{6}$$

where the prefactor $\mathcal{Q}_{Z'}$ is defined as

$$\mathcal{Q}_{Z'}(T) = 1 - \frac{\sqrt{2}}{G_F}\frac{Q_{Z'}}{Q_{\mathrm{SM}}}\frac{g_{Z'}^{\nu V}}{2M_N T + M_{Z'}^2}. \tag{7}$$

The corresponding modified nuclear charge $Q_{Z'}$ associated to the $Z^{'}$ can be further realized as related to the quark coupling

$$Q_{Z'} = \left(2g_{Z'}^{uV} + g_{Z'}^{dV}\right)Z + \left(g_{Z'}^{uV} + 2g_{Z'}^{dV}\right)N. \tag{8}$$

Taking into account the universal coupling of leptons and quarks, it becomes

$$Q_{Z'} = 3g_{Z'}\left(N + Z\right). \tag{9}$$

Accordingly, Eq. (7) scales as $g_{Z'}^2$, resulting in a proportionality of up to $g_{Z'}^4$ in the cross section of Eq. (6). Equation (7) stresses that there is a possibility of destructive interference with $Z^{'}$, causing suppression to the cross section, originating from a negative coupling, which gives rise to a valley in the exclusion plot [10]. However, despite its visibility within the COHERENT exclusion limits, it is beyond the sensitivity reach of the current reactor-based experiments [10, 82] with the exception of DRESDEN-II [69].

It is noteworthy that this $Z^{'}$ mediator model is in principle related to NSI vector interaction which will be discussed later in Sect. 2.2.1. Our discussion here, however, pertains to light $Z^{'}$ mediator model, where momentum transfer is considerably larger compared to the mediator mass [10], therefore we discuss the two models separately.

2.1.2. Light scalar mediator

As in BSM framework, CEνNS can be modified via a possible scalar propagator, thus the SM is extended in this study to include a real light scalar boson ϕ with mass M_ϕ. We adopt a simple CP-even mediator model in which the new interactions of ϕ with neutrinos and quarks arise from the Lagrangian [40]

$$\mathcal{L}_{\phi} = \phi\left(g_{\phi}^{qS}\bar{q}q + g_{\phi}^{\nu S}\bar{\nu}_R\nu_L + H.c.\right) - \frac{1}{2}M_{\phi}^2\phi^2, \tag{10}$$

where g_{ϕ}^{qS} and $g_{\phi}^{\nu S}$ represents the scalar-quark and scalar-neutrino couplings, respectively.

The ϕ interaction's contribution to the cross section of CEνNS combines in an incoherent manner with the SM cross section [40, 80]

$$\frac{d\sigma_{\mathrm{SM}+\phi}}{dT} = \frac{d\sigma_{\mathrm{SM}}}{dT} + \frac{d\sigma_{\phi}}{dT}, \tag{11}$$

with

$$\frac{d\sigma_{\phi}}{dT} = \frac{M_N}{4\pi} g_{\phi}^{\nu S^2} \mathcal{Q}_{\phi}^2 \left(\frac{M_N T}{E_{\nu}^2 (M_{\phi}^2 + 2M_N T)^2} \right) F^2(q^2). \tag{12}$$

The nuclear charge associated with the exchange of the ϕ can be given by [80]

$$\mathcal{Q}_{\phi} = Z \sum_{q=u,d} g_{\phi}^{qs} \frac{m_p}{m_q} f_q^p + N \sum_{q=u,d} g_{\phi}^{qs} \frac{m_n}{m_q} f_q^n, \tag{13}$$

where $m_{p,n}$ and m_q represents the mass of nucleon [proton (p), neutron (n)] and quarks (u, d). The hadronic form factors $f_{u,d}^{p,n}$ establish the effective low-energy coupling between a ϕ mediator and the nucleon (p, n) for the quark q [40, 83], and their latest updated values are [84, 85]

$$f_u^p = (20.8 \pm 1.5) \times 10^{-3},$$
$$f_u^n = (18.9 \pm 1.4) \times 10^{-3},$$

For simplicity, we assume a universal coupling to leptons and quarks, resulting in

$$\mathcal{Q}_{\phi} = g_{\phi}\ 17.3\ (N + Z). \tag{14}$$

As a result, we can work within the M_{ϕ} and g_{ϕ} parameter space, and it is evident that the relevant part of the cross section (Eq. 12) scales with g_{ϕ}^4 as well.

As the scalar-neutrino interaction does not preserve the chirality of the particles involved, thus no interference can be expected with the SM Z-boson interactions that conserve chirality. Therefore, there is no possible allowed space within the exclusion plot, contrary to the light $Z^{'}$ mediator case. Moreover, both $Z^{'}$ and ϕ mediators are being investigated to explain the observed 4.2σ deviation from SM prediction of anomalous magnetic moment of μ (possibly due to new physics BSM) observed by BNL and Fermi lab [80, 86–88].

It is noteworthy to mention that, in investigations of neutrino-nucleus scattering, both of these models are intriguing because the mediators may affect the recorded recoil spectra, particularly when their masses are below the maximum momentum transfer [9]. As a result, experiments employing reactor neutrinos can exhibit even greater sensitivity, particularly in the mediator mass region below ~ 10 MeV, outperforming experiments utilizing π-DAR sources.

2.2. Non-standard interactions

NSIs are an extension of the neutral current with four-fermion operators in the neutrino-quark sector and can be used to probe various BSM neutrino physics scenarios independent of models, typically assuming new mediators much heavier than those in the SM gauge bosons [46]. Accordingly, the new couplings are defined analogously to weak interactions at low energies in terms of G_F, since the heavy mediators are conventionally integrated out. The new couplings, in general, can be flavor-preserving $\epsilon_{\alpha\alpha}$ and/or flavor-violating, $\epsilon_{\alpha\beta}$ with $\alpha \neq \beta$, where symbols $\alpha,\beta \equiv [e, \mu, \tau]$ represents the lepton flavor indices. A deeper understanding of these new neutrino interactions is important, since they may affect neutrino oscillations [89] or even other branches of physics such as cosmology [90] and astrophysics [91, 92]. It is possible to study NSIs since they enter the SM CEνNS cross section through a modified or additional nuclear charge.

Moreover, in this article, we characterize the NSI contribution using a typical phenomenological description, assuming a four-fermion approximation (momentum transfer much smaller than the mediator's mass) for neutrino NSI with u and d quarks. When the momentum transfer in NSIs is significantly smaller than the mediator mass, the mediator can be integrated out, simplifying the interaction description [10, 42, 46]. This implies that for a lighter mediator, its influence on the scattering process becomes weaker.

2.2.1. *Vectorial interaction*

A major objective of this work is to examine potential deviations from the SM CEνNS expectations. Novel interactions involving neutral currents are usually addressed in the form of vector NSIs resulting from the four-fermion operators [40, 42]

$$\mathcal{O}_{\alpha\beta}^{qV} = \left(\bar{\nu}_{\alpha}\gamma^{\mu}L\nu_{\beta}\right)\left(\bar{q}\gamma_{\mu}Pq\right) + \mathrm{h.c.}, \tag{15}$$

where $q \equiv [u, d]$ represents the first generation quark and $P \equiv [L, R]$ denotes the left- or right-handed chiral projection operator. It is evident that this vector-type interaction exhibits the similar structure as the conventional SM CEνNS, which enables the couplings to quarks can be directly absorbed in weak charges ($Q_{\mathrm{SM}} \rightarrow \mathcal{Q}_{\mathrm{NSI}}^V$). In addition, the operator in Eq. (15) may also induce a flavor change among the neutrinos involved, so contrary to the SM case, within this framework the CEνNS cross section might become flavor-dependent. It is possible to express the NSI charge or modified weak charge in its most general form as

$$\mathcal{Q}_{\mathrm{NSI}}^V = \left[\left(2\epsilon_{\alpha\alpha}^{uV} + \epsilon_{\alpha\alpha}^{dV} + g_p^V\right)Z + \left(2\epsilon_{\alpha\alpha}^{dV} + \epsilon_{\alpha\alpha}^{uV} + g_n^V\right)N\right] + \sum_{\alpha\beta}\left[\left(2\epsilon_{\alpha\beta}^{uV} + \epsilon_{\alpha\beta}^{dV}\right)Z + \left(2\epsilon_{\alpha\beta}^{dV} + \epsilon_{\alpha\beta}^{uV}\right)N\right], \tag{16}$$

where the interactions that preserve flavor including SM CEνNS are represented by the first part within the bracket and the interactions that change flavor are represented by the second part. It is evident that, in the absence of flavor independent ($\epsilon^{uV}_{\alpha\alpha}$, $\epsilon^{dV}_{\alpha\alpha}$) and dependent ($\epsilon^{uV}_{\alpha\beta}$, $\epsilon^{dV}_{\alpha\beta}$) NSI couplings, this Eq. (16) will return to the case of SM CEνNS (Eq. 2).

For vector NSIs, it is only possible to probe effective electron-type couplings such as ϵ^{uV}_{ee} and ϵ^{dV}_{ee} with reactor neutrinos. However, it is still possible to investigate a wide range of couplings − flavor preserving as well as altering, both, with π-DAR beams as they also contain ν_μ & $\bar{\nu}_\mu$. Studies of such couplings have already produced bounds for any two parameter space that keeps other couplings zero at a time [23, 40, 93].

2.2.2. *Tensorial interaction*

A generalization of vectorial NSIs can result in NSIs of tensor type [94], which occurs naturally in the neutrino generalized interactions (NGIs) [62, 95]. New NSIs of tensor type may arise between neutrinos and quarks as a result of considering operators of the form [94, 96]

$$\mathcal{O}^{qT}_{\alpha\beta} = \left(\bar{\nu}_\alpha \sigma^{\mu\nu} \nu_\beta\right) + \left(\bar{q}\sigma_{\mu\nu} q\right) + \text{h.c.}\,, \tag{17}$$

where the symbols q, α, and β have the same meanings as previously described. Since the tensorial NSIs violates chirality conservation, destructive interference with SM CEνNS is not possible. This interaction opens up a large window to probe new interactions beyond the SM at low energies, as well as the possibility that tensorial NSIs are associated with neutrino's electromagnetic properties [97]. It is possible to combine the corresponding couplings to quarks into a new modified nuclear charge which is in resemblance to the weak charge in the CEνNS cross section and can be expressed as

$$\mathcal{Q}^{T}_{\text{NSI}} = \left(2\epsilon^{uT}_{\alpha\beta} + \epsilon^{dT}_{\alpha\beta}\right)Z + \left(\epsilon^{uT}_{\alpha\beta} + 2\epsilon^{dT}_{\alpha\beta}\right)N. \tag{18}$$

As opposed to the SM case, here as well as other BSM models, the proton number is not weighted with a small prefactor, which means that the cross section does not necessarily scale with the characteristic dependence on the squared neutron number. It is possible for flavor-changing tensorial NSIs to exist and are tested at π-DAR sources [40]. However, the reactor sites can only probe electron flavor couplings due to $\bar{\nu}_e$ source. As a result, we focus on flavor-diagonal couplings (ϵ^{uT}_{ee} and ϵ^{dT}_{ee}) in this analysis.

The SM CEνNS cross section is modified within this framework and the new tensorial NSIs simply adds to the conventional CEνNS cross section, resulting in,

$$\frac{d\sigma_{\text{SM+T(NSI)}}}{dT} = \frac{d\sigma_{\text{SM}}}{dT} + \frac{4G_F^2}{\pi} {\mathcal{Q}^{T}_{\text{NSI}}}^2 M_N \left(1 - \frac{M_N T}{4E_\nu^2}\right). \tag{19}$$

It is essential to emphasize that the distinct kinematic factors in the CEνNS cross section of Eqs. (1) and (19) enable the tensorial NSIs signal to expand to higher energy ranges. It is also evident from Eq. (19) that, owing to its distinct structure compared to vectorial interaction, there is no potential for destructive interference. As a result, tensorial interactions are more stringent compared to the vectorial case.

3. Event rate in TEXONO

Each of the four interactions has been described in Sect. 2 with their physics cross section. The SM CEνNS cross section will be modified by the vector interaction term for low mass vector mediator and vector NSIs cases, whereas the interaction cross section will be simply added to the SM CEνNS cross section for low mass scalar mediator and tensorial NSIs. As a result of knowing these cross sections, we are able to calculate the corresponding CEνNS signal from reactor neutrinos. In terms of the nuclear recoil energy T, the differential recoil spectrum can be obtained as,

$$\frac{dR}{dT} = N_T \int \frac{d\sigma}{dT}\frac{d\phi}{dE_{\bar{\nu}_e}} dE_{\bar{\nu}_e}, \tag{20}$$

where N_T, $d\sigma/dT$, and $d\phi/dE_{\bar{\nu}_e}$ represents the number of nuclei in the detector, the CEνNS differential cross section (as illustrated in Sect. 2), and the reactor neutrino flux as a function of energy $E_{\bar{\nu}_e}$, respectively.

As the TEXONO experiment utilizes HPGe detector technology operated at liquid nitrogen temperature, the associated signal is collected in the from of ionization energy produced by the nuclear recoil. Whenever a nuclear recoil occurs inside the detector, part of its energy induces ionization in the material and the rest contributes to the increase in thermal energy. As a result of this ionization, charge carriers (electrons and holes) are created in the detector and collected by electrodes as signals. The ionization produced by a recoiling nucleus is typically lower than that produced by an electron of the same energy due to differences in mass, interaction cross section, velocity, and quantum properties [98–100]. This loss in energy can be taken into account by using the dimensionless ionization quenching factor $Q(T)$, defined as the ratio of ionization energy produced by nuclear recoils and that produced by electron recoils of equal energy

$$Q(T) = \frac{E_{ee}}{T}, \tag{21}$$

where symbol E_{ee} represents the electron equivalent ionization energy. Measurements of the $Q(T)$ for nuclear recoils have been extensively performed [66, 101] and its energy dependence predicted by Lindhard is observed [104]. The $Q(T)$ in the standard Lindhard model is defined as

$$Q(T) = \frac{kg(T)}{1 + kg(T)}, \tag{22}$$

where $g(T)$ is a function of recoil energy, and k is a dimensionless parameter, which is a measure of the electronic energy loss. Based on these considerations, it is possible to write the differential event rate (ionization energy spectrum) in terms of the differential recoil energy spectrum as

$$\frac{dR}{dE_{ee}} = \frac{dR}{dT} \times \frac{dT}{dE_{ee}} \equiv \frac{dR}{dT} \times \frac{1}{\left(Q + T\frac{dQ}{dT}\right)}. \tag{23}$$

In Eq. (23), differential event rates are calculated assuming an infinitely good energy resolution for the detector. However, due to the finite energy resolution of a detector, the observed differential energy spectrum will be smeared in practice. Considering a Gaussian detector response, the differential event rate with measurable energy E_M convoluted with the detector energy resolution can be expressed as

$$\frac{dR}{dE_M} = \frac{\int_0^\infty R(E_{ee}, E_M, \sigma)\frac{dR}{dE_{ee}}dE_{ee}}{\int_0^\infty R(E_{ee}, E_M, \sigma)dE_{ee}}, \tag{24}$$

where $R(E_{ee}, E_M, \sigma) = \frac{1}{\sqrt{2\pi\sigma^2}} \exp\left[\frac{-(E_M - E_{ee})^2}{2\sigma^2}\right]$ is the Gaussian nature of detector response. The standard deviation σ typically characterizes the energy resolution of the detector and can be written as $\sigma^2 = \sigma^2_{\rm RMS} + E_{ee}F\eta$, where F is the fano factor, η is the mean ionization energy required to produce an electron–hole pair, and $\sigma_{\rm RMS} = 49$ eV$_{\rm ee}$ (in our case, for nPCGe detector) is the RMS (Root-Mean-Square) energy resolution for test-pulser, which is ≡"Pedestal-Noise-Profile-RMS" [66].

4. Data sets and analysis method

The data sets used in the current BSM analysis were collected using a nPCGe detector confined within an anti-Compton (AC) detector NaI(Tl) of mass 38.3 kg installed inside Kuo-Sheng neutrino laboratory's 50 ton shielded structure with cosmic-ray (CR) veto scintillator panels. As a result of the low threshold of 300 eV$_{ee}$ of the nPCGe detector, as well as the absence of anomalous surface events, data collected with this detector are selected for the present analysis. A comprehensive explanation of the background modeling used in the TEXONO data analysis, including the associated systematics and uncertainties, is thoroughly discussed in Refs. [66, 105, 106]. In our data filtration, advanced data-driven modeling and Monte Carlo simulations are used to accurately account for background effects, thereby ensuring more reliable signal extraction [65, 106, 107].

Each Ge-trigger is classified by AC$^{+(-)}\otimes$CR$^{+(-)}$, where the superscript "−" (minus) denotes anti-coincidence, and the superscript "+" (plus) denotes coincidence between the Ge-signals and the AC and CR detectors. The AC$^-\otimes$CR$^-$ events are independent of other active veto detector systems, making them potential candidates for neutrino, WIMPs (Weakly Interacting Massive Particles), and other exotic events [107]. The residual reactor (ON−OFF) spectrum of the AC$^-\otimes$CR$^-$ events is

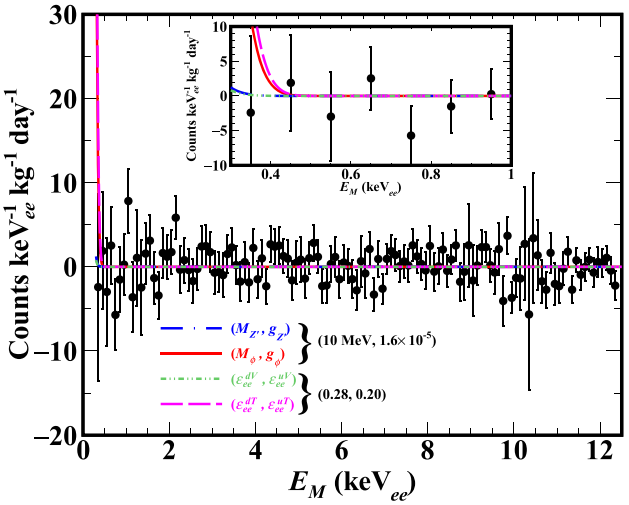

Fig. 1 The residual reactor (ON−OFF) spectrum of nPCGe with AC$^-\otimes$CR$^-$ selection and 300 eV$_{ee}$ detection threshold [105]. Theoretical rates for representative light mediator models with a mass of 10 MeV and a coupling strength of 1.6×10^{-5} are overlaid onto the experimental data. The specified coupling strength of 1.6×10^{-5} is excluded at the 90% C.L. for a 10 MeV scalar mediator, whereas, for the same mediator mass and coupling value, it is not excluded at the 90% C.L. for a vector mediator. Accordingly, this particular coupling at the same mass shows that for a scalar mediator, the relevant cross section component scales inversely with recoil energy. In contrast, for a vector mediator, it scales with the inverse square of the recoil energy, resulting in a less pronounced signal. Similarly, theoretical rates for vectorial as well as tensorial NSIs with $\epsilon_{ee}^{u[T,V]} = 0.20$ and $\epsilon_{ee}^{d[T,V]} = 0.28$ are also superimposed onto the experimental data. In NSIs, the application of these two identical positive couplings is intended to demonstrate the enhancement observed in both vectorial and tensorial NSI cases. This reveals different properties due to the modified charge (Eqs. 16 and 18). For tensorial NSIs, there is a greater excess with the same coupling, attributed to its dependence on proton number

represented in Fig. 1 using 124.2 kg-days of reactor ON and 70.3 kg-days of reactor OFF data adopted for the present analysis. In the sub-keV region (the region of interest) of the TEXONO data, the absence of any excess events above the observed background suggests compatibility with the background-only hypothesis. Consequently, we established the upper limits.

In the physics analysis we have used the classical statistical approach to evaluate the statistical significance of our considered theoretical models. Accordingly, our definition for the χ^2 is

$$\chi^2 = \sum_i \left(\frac{N_i - (1+\alpha)\mu_i}{\sigma_i} \right)^2 + \left(\frac{\alpha}{\sigma_\alpha} \right)^2, \tag{25}$$

where N_i and σ_i are the experimentally observed counts and corresponding uncertainty in the ith bin, respectively. In the absence of a definitive signal of new physics, N_i and σ_i are obtained from the energy spectrum of uncorrelated filtered events shown in Fig. 1, with the measured data treated as background to derive the limits. Symbol μ_i represents the theoretical prediction in the ith bin corresponding to the considered low mass mediators and NSIs estimated according to Eq. 24. Uncertainty in the flux normalization σ_α is considered to be 5%. We fit 7 bins of measured energy spectra (Fig. 1) in the energy region from (0.3 to 1.0) keV$_{\rm ee}$ to obtain the χ^2_{min} taking into account the nuisance parameter α. After searching the χ^2_{min} using Eq. 25, we measured $\Delta\chi^2 = \chi^2(x) - \chi^2_{min}$ to evaluate the limit of considered BSM physics parameters, where x is the considered new physics parameter. To perform the analysis at 90% C.L. for low mass mediator for each mass the limit was estimated by varying the respective coupling. Thus, for low mass mediators it is a one-dimensional problem whereas for NSIs this is treated as a two-dimensional problem.

5. Results and discussions

A crucial point to consider in sub-keV physics analysis is the $Q(T)$ for nuclear recoil energies up to keV, which contributes the largest uncertainty. This $Q(T)$ is highly relevant to CEνNS and low mass DM searches in this energy range. Hitherto, the most stringent limit on $Q(T)$ has been obtained from CEνNS measurements on Lindhard $k < 0.260$, conducted as part of the νGEN collaboration [11]. Recent $Q(T)$ measurements down to sub-keV energy region were also constrained by the CONUS collaboration [101]. These measurements, in conjunction with References [102, 103], demonstrate a notable deviation and impose challenges to the standard Lindhard model, especially in the context of $T < 1$ keV$_{nr}$. Therefore, for each explored physics scenario described in Sect. 2, we have considered three possible cases for $Q(T)$ effect: conservative, intermediate, and optimistic. We consider k values (associated with $Q(T)$ as in Eq. 22) for conservative (0.157 − theoretical prediction for Germanium in the Lindhard model), intermediate (0.200), and optimistic scenarios (0.260), respectively, to cover the range of presently preferred values. In the following subsections, we illustrate our results for light mediator models and NSIs that take into account these ranges of k values.

Prior to investigating BSM aspects, we set an upper limit at 90% C.L. on the observed CEνNS events, in view of the absence of any clear excess at low energy in the measured spectrum for the SM expected CEνNS events, for the sake of completeness. The upper limit is presented in Table 1 for the chosen benchmark k values. In establishing these limits, we utilized a minimum χ^2 analysis, as discussed in Sect. 4, to explore the excess in view of SM prediction for selected benchmark k values within the signal region of 300 eV$_{ee}$ to 1000 eV$_{ee}$ in the residual spectrum. It is apparent that our current limits lack significant robustness in light of the 300 eV$_{ee}$ achieved threshold. Nonetheless, we anticipate that advancements in the threshold in the near future could lead to either the detection of an excess of events or the imposition of stringent constraints on the SM predicted CEνNS events.

5.1. Constraints on low mass mediator

Reactor-based experiments exhibit greater sensitivity to light mediators with masses below a few tens of MeV, primarily owing to the abundance of low-energy neutrino flux they offer. Conversely, for larger masses of light mediator, the constraints set by reactor-based experiments are less rigorous than those derived from COHERENT, as the latter involves higher nuclear recoil energy generated by neutrinos from the SNS. As shown in Fig. 2, the derived limits in the current work demonstrate this behavior and are compared to those from the other reactor-based experiments and COHERENT (CsI and Ar).

In Fig. 2a, for *vector light mediator*, our investigation spans the $(m_{Z'}, g_{Z'})$ parameter space, ultimately reaching a coupling strength $g_{Z'}$ of $\mathcal{O}(10^{-5})$. This exploration predominantly focuses on the $m_{Z'}$ range below 10 MeV for the chosen set of k values. The limits we have obtained are comparable, thus confirming the constraints observed in other contemporary reactor-based experiments, such as DRESDEN-II [69], CONUS [10], and CONNIE [8], across both the low and high $m_{Z'}$ regions. In contrast, for the high $m_{Z'}$ region, our findings, along with those of other reactor-based experiments, exhibit less stringency when compared

Table 1 The SM signal predictions and experimental constraints from the TEXONO data are summarized for the selected conservative, intermediate, and conservative k values

k values in the Lindhard model	SM signal prediction (Counts keV$_{ee}^{-1}$ kg^{-1} day^{-1})	Achieved limit at 90% C.L. (Counts keV$_{ee}^{-1}$ kg^{-1} day^{-1})
0.157	0.132	16.2
0.200	0.508	17.0
0.260	1.55	18.6

to the limits established by COHERENT [4]. As an illustrative example, the 90% C.L. exclusion for the coupling $g_{Z'}$ at a $m_{Z'}$ of 10 MeV is estimated to be in the range of (7.1 to 4.0)$\times 10^{-5}$, considering both conservative and optimistic sets of k values, as depicted in Fig. 2a. The corresponding $\Delta\chi^2$ distributions to get the essence of the derived limits are displayed in Fig. 2b. Additionally, we agree with the measurements of References [8, 108], and have ruled out the possibility of universal $Z^{'}$ mediators can provide explanation to the observed anomalous magnetic moments $(g-2)_{\mu}$ of the muon. The presence of the "island of non-exclusion" in the COHERENT [CsI and Ar] limits is attributed to destructive interference (see Eq. 7), and this peculiar feature is absent from the limits of TEXONO, CONNIE and CONUS reactor-based experiments (with the exception of DRESDEN-II [69]) as they have not yet achieved the requisite sensitivity to observe this phenomenon.

The *light scalar mediator* exclusion region in the (M_ϕ, g_ϕ) plane at 90% C.L. from the TEXONO data considering an optimistic to conservative set of k values is shown in Fig. 2c along with concurrent reactor-based and COHERENT [CsI and Ar] experiments. It is evident from Fig. 2c that with the current analysis we (along with other reactor-based experiments) excluded COHERENT [CsI and Ar] limits for scalar light mediators with $M_\phi < 10$ MeV. The contribution of light scalar mediator to the event rate is proportional to $g_\phi^{\nu S^2}/(M_\phi^2 + 2M_N T)$ in this case according to Eq. 12. In the case of low M_ϕ, the contribution of scalar mediators to the rate is dependent only on the coupling g_ϕ, whereas for heavy M_ϕ, it is dependent on the g_ϕ/M_ϕ ratio. A visual representation of these two cases are evident in Fig. 2c. As an illustration, for $M_\phi = 10$ MeV, the 90% C.L. limit on the strength of g_ϕ varies within the range of (1.6−0.93)$\times 10^{-5}$, considering the assumed range of k values from conservative to optimistic. For reference, their respective $\Delta\chi^2$ distributions are displayed in Fig. 2d.

The achieved limits for scalar mediator are more stringent than those of a vector mediator. This characteristic emerges from the cross section formulations (Eqs. 11 and 6). In the case of a vector mediator, the cross section (Eq. 6) is inverse square proportional to the T, while for a scalar mediator (Eq. 11), it scales as the inverse of the T. This leads to a steeper rate and, consequently, more stringent limits in the case of a scalar mediator compared to a vector mediator, particularly in low mass region. This distinctive feature can be visually comprehended by referring to Fig. 1. In Fig. 1, we have presented the theoretical spectra (superimposed on the TEXONO data) for both scalar and vector mediators with identical mass and coupling strengths. It exhibits a steeper curve in the case of the scalar mediator in comparison to the vector mediator.

The detection threshold, background level, and measurement uncertainty significantly impact the sensitivity of our limits. The TEXONO data demonstrate that the uncertainty of residual spectrum is crucially affecting our limits at the achieved threshold of 300 eV$_{ee}$ with controlled background. This is attributed to the lower statistics of the reactor OFF data, which constitutes the pure background in reactor experiments, comprising various known and unknown background components such as γ-rays, neutrons, cosmic events, cosmogenic events, etc., similar to the reactor ON data, except for the absence of signal $\bar{\nu_e}$. The reactor OFF data, totaling 70.3 kg-days, has statistics approximately 1.8 times lower than that of the reactor ON data, which amounts to 124.2 kg-days. This leads to a marked increase in the size of the error bars, signifying a greater level of uncertainty within the residual spectrum. Improving the statistics of reactor OFF data and lowering the threshold are the primary objectives of our ongoing projects, aiming to increase sensitivity if no clear signature of excess in the event rate is observed.

5.2. Constraints on non-standard interactions

Reactor neutrino experiments face limitations in the exploration of different NSIs parameters because they rely on a single flavor neutrino flux, in contrast to the three flavors available at the π-DAR source. The limits achieved with TEXONO data in the present analysis for vectorial and tensorial NSIs are presented in Fig. 3. Attributing to low detection threshold and signal's broader reach in

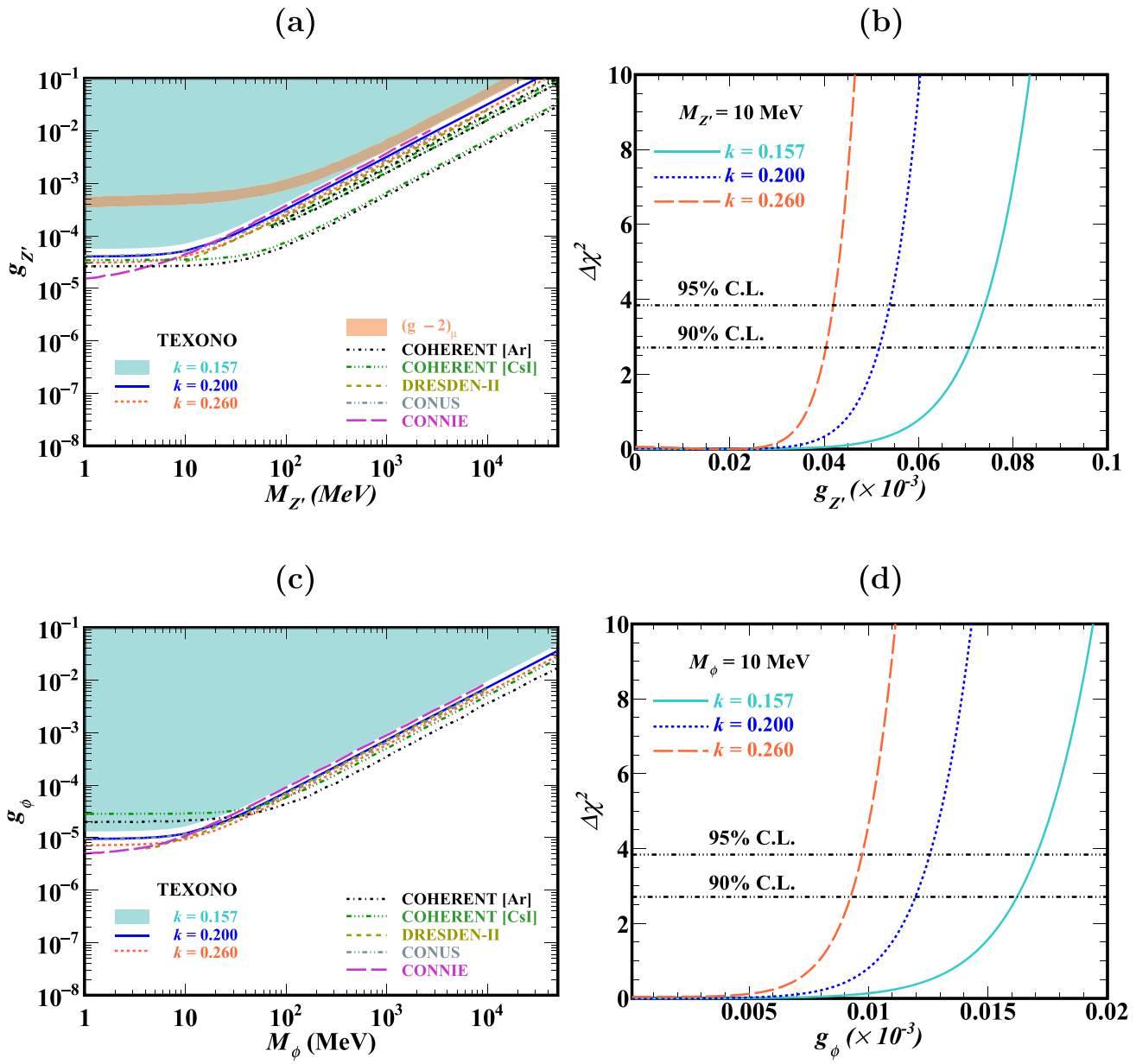

Fig. 2 The 90% C.L. exclusion plots obtained from TEXONO are as follows: (**a**) For scalar mediators in the (M_ϕ, g_ϕ) plane; (**b**) The corresponding $\Delta\chi^2$ distribution, considering a range of k values, at M_ϕ =10 MeV; (**c**) For vector mediators in the $(M_{Z'}, g_{Z'})$ plane; (**d**) The corresponding $\Delta\chi^2$ distribution, considering a range of k values, at $M_{Z'}$ =10 MeV. We have superimposed the results from multiple experiments, including the CONNIE at 95% C.L. [8], the DRESDEN-II findings at 2σ C.L. [69], the COHERENT observations at 90% C.L. [4], and the CONUS results at 90% C.L. [10], to provide an overview of the current status, refraining from direct comparisons due to differences in chosen C.L., particularly with CONNIE and DRESDEN-II. We have represented the achieved limits at 95% C.L. for $(M_\phi, M_{Z'}) \equiv 10\ MeV$ by displaying the corresponding line in both figures (**b**) and (**d**), alongside the existing limits at 90% C.L

comparison to SM CEνNS, we place the competitive bounds, in particular, for tensorial NSI couplings ϵ_{ee}^{uT} and ϵ_{ee}^{dT}.

In the case of the vectorial NSIs scenario, it shares a similar chiral structure to the SM case, implying the same kinematic cutoff. The associated bounds can be observed in Fig. 3a, demonstrating a pronounced dependence on $Q(T)$. This dependence arises because $Q(T)$ notably impacts the expected number of signal events within the region of interest. These bounds are relatively less stringent, primarily owing to the limitations of current experimental sensitivity. However, future experimental improvements in terms of detection threshold and reducing background levels may enhance the potential for detecting CEνNS, which would also considerably boost the sensitivity to vectorial NSIs.

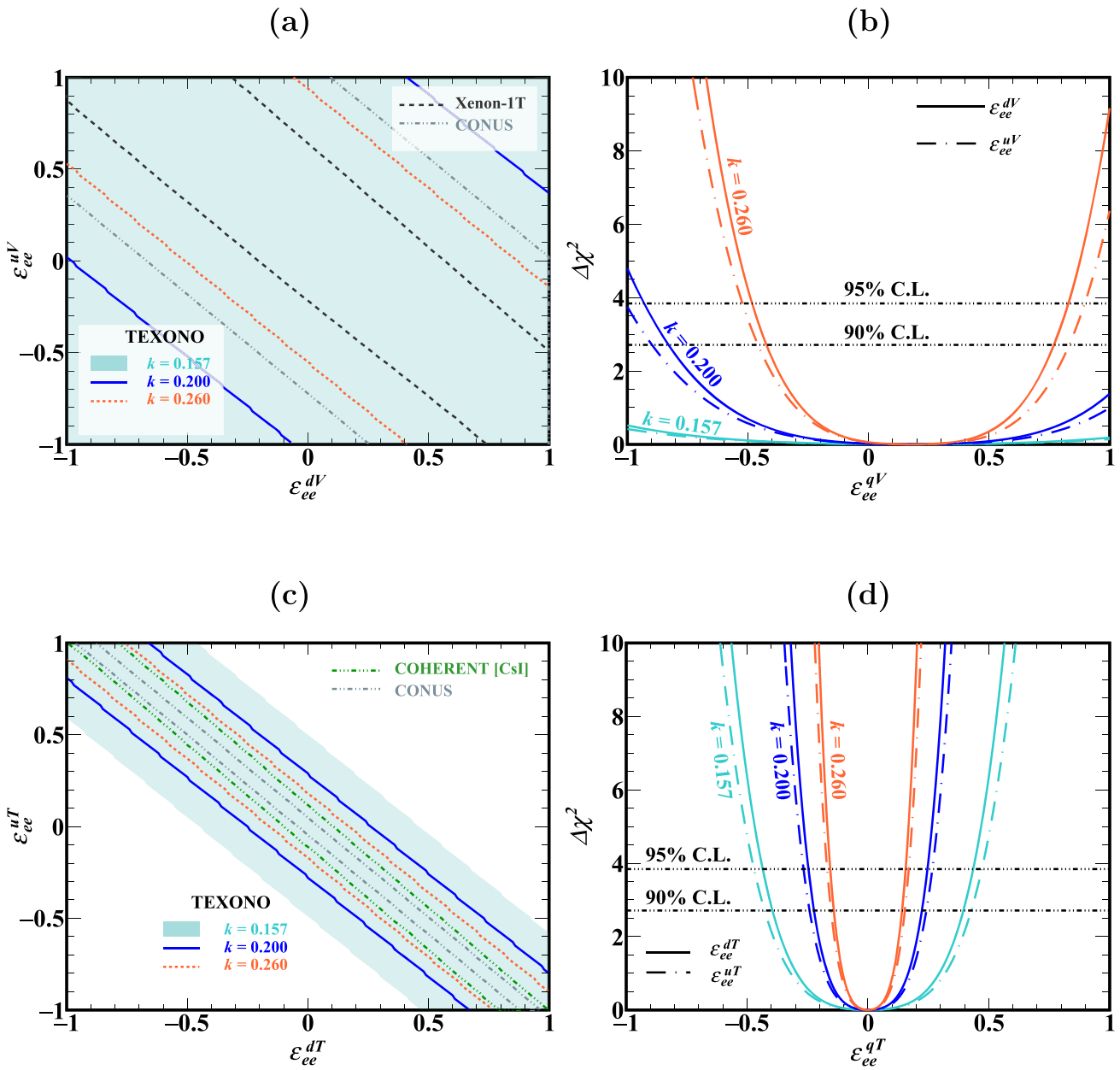

Fig. 3 The 90% C.L. allowed shaded regions based on TEXONO *n*PCGe data are depicted in: (**a**) The $(\epsilon_{ee}^{dV}, \epsilon_{ee}^{uV})$ space; (**b**) The corresponding $\Delta\chi^2$ distribution, considering a range of k values, and with one parameter set to zero at a time; (**c**) The $(\epsilon_{ee}^{dT}, \epsilon_{ee}^{uT})$ space; (**d**) The corresponding $\Delta\chi^2$ distribution, considering a range of k values, and with one parameter set to zero at a time. In order to provide a comprehensive view, we have superimposed the most recent constraints obtained from other experiments, including the 90% C.L. results from CONUS [10], XENON 1T [109], and COHERENT [93], facilitating comparison with our findings. Additionally, for completeness, we have depicted the attained limits at 95% C.L. by illustrating the corresponding line in both figures (**b**) and (**d**), alongside the existing limits at 90% C.L

In the case of tensorial NSIs, the predicted spectrum includes a tail that extends to relatively higher energies. Because of this distinct characteristic, our bounds on tensorial NSIs are more competitive within the coupling space when compared to the vectorial case, as demonstrated in Fig. 3c. This feature is also evident in Fig. 1, which illustrates that, for equivalent coupling strengths, tensorial NSIs benefit from a wider energy range in the rate when compared to vectorial NSIs.

Here, we also examine the impact of varying Lindhard k values from conservative to optimistic cases in the process of deriving limits, as demonstrated in Fig. 3a and c. In these figures, the parameter space is treated as a two-dimensional case for χ^2 analysis. On the other hand, in the

case of $\Delta\chi^2$ distributions, as depicted in Fig. 3b and d, the dashed line at the 90% C.L. is displayed for the one dimensional scenario, where one parameter is set to be zero at a time. The attained 90% C.L. limits for the conservative scenario in ϵ_{ee}^{uT} and ϵ_{ee}^{dT} are within the range of $(-0.43$ to $0.43)$ and $(-0.39$ to $0.39)$, respectively.

6. Conclusions

The TEXONO experiment aims to detect CEνNS with point contact HPGe detectors at the Kuo-Sheng nuclear power plant in Taiwan. In the present work, we examined the probable physics aspects that could impact the detection of CEνNS and tried to constrain them based on TEXONO's nPCGe data (with analysis threshold of 300 eV_{ee}), in particular NSIs within the neutrino-quark sector, as well as light vector and scalar mediators. As simplified models, the latter two have been tested for their impact on CEνNS. A standard χ^2 analysis procedure is implemented to evaluate statistical significance of these models and constrain their mass and coupling strength.

The most uncertain factor in TEXONO is $Q(T)$, which is the least known input parameter. In conjunction with neutrino energies below 8 MeV, uncertainty in the $Q(T)$ makes CEνNS measurements at reactor sites even more challenging. As a result, we derive the BSM constraints for three different quenching parameters, $k=(0.157, 0.200, 0.260)$, where k corresponds to the $Q(T)$ (Eq. 22). In the conservative (0.157), intermediate (0.200), and optimistic (0.260) scenarios, these values of k span the range of currently favored values. In the interest of completeness, before delving into the exploration of BSM aspects, an upper limit at 90% C.L. was set on the observed CEνNS events at these benchmark k values, in the lack of any clear excess at low energy in the measured spectrum for the SM expected CEνNS events. The current limits within this framework are evidently lacking in robustness and require improvement in both the threshold ($<$ 300 eV_{ee}) and the reduction of uncertainty in the residual spectrum.

In the present analysis, TEXONO benefits from the low energies of reactor neutrinos, allowing it to establish stringent constraints on light vector and scalar mediators that interact with both neutrinos and quarks, as well as vectorial and tensorial NSIs within the neutrino-quark sector. While our limits from reactor neutrinos are less robust for larger mediator masses when compared to π-DAR source COHERENT experiment, this is primarily because the available neutrinos in reactor experiments have lower energy ($<$8 MeV). This allows us to benefit from encompassing the full coherency regions, which is a limitation in π-DAR source. Our present constraints on both light vector and scalar mediators are in line with those observed in other reactor-based experiments.

With the recent achievement of a low-energy detection threshold, reactor-based experiments have become valuable tools for investigating NSIs in the sub-keV energy regime, where the distinctive signatures of such physics phenomena are most prominent. The limits obtained in the current analysis for both vectorial and tensorial NSIs are comparatively less stringent. Consequently, there is still potential for further improvement in the near future, especially with the development of a detection threshold < 150 eV_{ee} and reduction in the background levels. Detailed studies of different background channels, development in the detection threshold (at the software as well as hardware levels), and energy resolution are themes of our ongoing research efforts. Since the determination of these limits relies heavily on $Q(T)$, enhancing both the experimental measurements and the theoretical predictions of $Q(T)$ can be a viable solution to this issue. Such improvements will enhance the robustness of sub-keV physics analyses in the coming future.

Acknowledgements This work is supported by the Academia Sinica Principal Investigator Award AS-IA-106-M02, contracts 106-2923-M-001-006-MY5, 107-2119-M-001-028-MY3 and 110-2112-M-001-029-MY3, from the Ministry of Science and Technology, Taiwan, and 2021/TG2.1 from the National Center of Theoretical Sciences, Taiwan.

References

[1] D Z Freedman *Phys. Rev. D* **9** 1389 (1974) https://doi.org/10.1103/PhysRevD.9.1389
[2] D Baxter et al *JHEP* **02** 123 (2020) https://doi.org/10.1007/JHEP02(2020)123
[3] D Akimov et al *Science* **357** 1123 (2017) https://doi.org/10.1126/science.aao0990
[4] M Cadeddu et al *JHEP* **01** 116 (2021) https://doi.org/10.1007/JHEP01(2021)116
[5] D Akimov et al *Phys. Rev. Lett.* **126** 012002 (2021) https://doi.org/10.1103/PhysRevLett.126.012002
[6] J Colaresi et al *Phys. Rev. Lett.* **129** 211802 (2022) https://doi.org/10.1103/PhysRevLett.129.211802
[7] H T Wong et al Nuc. Phys. B - Proceedings Supplements **221**, 320 (2011) https://www.sciencedirect.com/science/article/pii/S0920563211007146
[8] A Aguilar Arevalo et al *Phys. Rev. D* **100** 092005 (2019) https://doi.org/10.1103/PhysRevD.100.092005
[9] H Bonet et al *Phys. Rev. Lett.* **126** 041804 (2021) https://doi.org/10.1103/PhysRevLett.126.041804
[10] H Bonet et al *JHEP* **5** 085 (2022) https://doi.org/10.1007/JHEP05(2022)085
[11] I Alekseev et al *Phys. Rev. D* **106** L051101 (2022) https://doi.org/10.1103/PhysRevD.106.L051101
[12] D Y Akimov et al *JINST* **15** P02020 (2020) https://doi.org/10.1088/1748-0221/15/02/P02020

[13] J Billard et al *J. Phys. G: Nucl. Part. Phys.* **44** 105101 (2017) https://doi.org/10.1088/1361-6471/aa83d0

[14] V Sharma et al *Phys. Rev. D* **103** 092002 (2021) https://doi.org/10.1103/PhysRevD.103.092002

[15] H T Wong et al *Phys. Rev. D* **75** 012001 (2007) https://doi.org/10.1103/PhysRevD.75.012001

[16] D Z Freedman et al *Ann. Rev. Nucl. Part. Sci.* **27** 167 (1977) https://doi.org/10.1146/annurev.ns.27.120177.001123

[17] S P Amanik et al *Phys. Rev. D* **75** 083008 (2007) https://doi.org/10.1103/PhysRevD.75.083008

[18] K G Balasi et al *Prog. Part. Nuc. Phys.* **85** 33 (2015) https://www.sciencedirect.com/science/article/pii/S0146641015000654

[19] M Biassoni et al *Astroparticle Phys.* **36** 151 (2012) https://www.sciencedirect.com/science/article/pii/S0927650512001132

[20] V Brdar et al *JCAP* **2018** 025 (2018) https://doi.org/10.1088/1475-7516/2018/04/025

[21] P Agnes et al *JCAP* **2021** 043 (2021) https://doi.org/10.1088/1475-7516/2021/03/043

[22] M Gerbino et al *Front. Phys.* **5** 70 (2018) https://www.frontiersin.org/articles/10.3389/fphy.2017.00070/full

[23] A N Khan et al *Phys. Rev. D* **100** 113003 (2019) https://doi.org/10.1103/PhysRevD.100.113003

[24] M Cadeddu et al *Phys. Rev. D* **101** 033004 (2020) https://doi.org/10.1103/PhysRevD.101.033004

[25] K Patton et al *Phys. Rev. C* **86** 024612 (2012) https://doi.org/10.1103/PhysRevC.86.024612

[26] M Cadeddu et al *Phys. Rev. Lett.* **120** 072501 (2018) https://doi.org/10.1103/PhysRevLett.120.072501

[27] P Coloma et al *JHEP* **08** 030 (2020) https://doi.org/10.1007/JHEP08(2020)030

[28] H S Lee *J. Univ. Sci. Tech. China* **46** 470 (2016) arXiv:1511.03783

[29] B C Canas et al *Phys. Lett. B* **784** 159 (2018) https://www.sciencedirect.com/science/article/pii/S0370269318305872

[30] X R Huang et al *Phys. Rev. D* **100** 071301 (2019) https://doi.org/10.1103/PhysRevD.100.071301

[31] G Fernandez-Moroni et al *JHEP* **03** 186 (2021) https://link.springer.com/article/10.1007/JHEP03(2021)186

[32] C Boehm et al *JCAP* **2019** 01 (2019) https://doi.org/10.1088/1475-7516/2019/01/043

[33] M C Gonzalez-Garcia et al *JHEP* **07** 019 (2018) https://doi.org/10.1007/JHEP07(2018)019

[34] D K Papoulias et al *Adv. High Energy Phys.* **2018** 6031362 (2018) https://www.hindawi.com/journals/ahep/2018/6031362/

[35] W Chao et al *JCAP* **2019** 010 (2019) https://doi.org/10.1088/1475-7516/2019/08/010

[36] D A Sierra et al *JCAP* **2022** 055 (2022) https://doi.org/10.1088/1475-7516/2022/01/055

[37] C A J O'Hare *Phys. Rev. D* **102** 063024 (2020) https://doi.org/10.1103/PhysRevD.102.063024

[38] J Monroe et al *Phys. Rev. D* **76** 033007 (2007) https://doi.org/10.1103/PhysRevD.76.033007

[39] A Gutlein et al *Astropart. Phys.* **34** 90 (2010) https://doi.org/10.1016/j.astropartphys.2010.06.002

[40] D K Papoulias et al *Phys. Rev. D* **97** 033003 (2010) https://doi.org/10.1103/PhysRevD.97.033003

[41] S Kerman et al *Phys. Rev. D* **93** 113006 (2016) https://doi.org/10.1103/PhysRevD.93.113006

[42] J Barranco et al *JHEP* **2005** 021 (2005) https://doi.org/10.1088/1126-6708/2005/12/021

[43] J Barranco et al *Phys. Rev. D* **76** 073008 (2007) https://doi.org/10.1103/PhysRevD.76.073008

[44] P Coloma et al *Phys. Rev. D* **96** 115007 (2017) https://doi.org/10.1103/PhysRevD.96.115007

[45] I Bischer et al *JHEP* **10** 096 (2018) https://doi.org/10.1007/JHEP10(2018)096

[46] P S Bhupal Dev et al *Sci. Post Phys. Proc.* **2** 001 (2019) https://scipost.org/10.21468/SciPostPhysProc.2.001

[47] C Giunti *Phys. Rev. D* **101** 035039 (2020) https://doi.org/10.1103/PhysRevD.101.035039

[48] P B Denton et al *JHEP* **04** 266 (2021) https://link.springer.com/article/10.1007/JHEP04(2021)266

[49] M Lindner et al *JHEP* **03** 097 (2017) https://doi.org/10.1007/JHEP03(2017)097

[50] P Vogel et al *Phys. Rev. D* **39** 3378 (1989) https://doi.org/10.1103/PhysRevD.39.3378

[51] C Giunti et al *Rev. Mod. Phys.* **87** 531 (2015) https://doi.org/10.1103/RevModPhys.87.531

[52] M Cadeddu et al *Phys. Rev. D* **98** 113010 (2018) https://doi.org/10.1103/PhysRevD.98.113010

[53] O G Miranda et al *JHEP* **07** 103 (2019) https://link.springer.com/article/10.1007/JHEP07(2019)103

[54] M Cadeddu et al *Phys. Rev. D* **102** 015030 (2020) https://doi.org/10.1103/PhysRevD.102.015030

[55] Y Farzan et al *JHEP* **05** 066 (2018) https://link.springer.com/article/10.1007/JHEP05(2018)066

[56] J B Dent et al *Phys. Rev. Lett.* **124** 211804 (2020) https://doi.org/10.1103/PhysRevLett.124.211804

[57] D A Sierra et al *JHEP* **294** 03 (2021) https://doi.org/10.1007/JHEP03(2021)294

[58] B Dutta et al *Phys. Rev. Lett.* **123** 061801 (2019) https://doi.org/10.1103/PhysRevLett.123.061801

[59] A Aguilar-Areval et al *JHEP* **04** 054 (2020) https://link.springer.com/article/10.1007/JHEP04(2020)054

[60] O G Miranda et al *Phys. Rev. D* **101** 073005 (2020) https://journals.aps.org/prd/abstract/10.1103/PhysRevD.101.073005

[61] J Billard et al *JCAP* (2018) https://doi.org/10.1088/1475-7516/2018/11/016

[62] D A Sierra et al *Phys. Rev. D* **98** 075018 (2018) https://doi.org/10.1103/PhysRevD.98.075018

[63] H T Wong *Int. J. Mod. Phys. A* **33** 1830014 (2018) https://doi.org/10.1142/S0217751X18300144

[64] M Deniz et al *Phys. Rev. D* **81** 072001 (2010) https://doi.org/10.1103/PhysRevD.81.072001

[65] A Sonay et al *Phys. Rev. C* **98** 024602 (2018) https://doi.org/10.1103/PhysRevC.98.024602

[66] A K Soma et al *NIM A* **836** 67 (2016) https://www.sciencedirect.com/science/article/pii/S0168900216308622

[67] P S Barbeau et al *JCAP* (2007) https://doi.org/10.1088/1475-7516/2007/09/009

[68] M Tanabashi et al *Phys. Rev. D* **98** 030001 (2018) https://doi.org/10.1103/PhysRevD.98.030001

[69] J Liao et al *Phys. Rev. D* **106** L031702 (2022) https://doi.org/10.1103/PhysRevD.106.L031702

[70] R H Helm *Phys. Rev.* **104** 1466 (1956) https://doi.org/10.1103/PhysRev.104.1466

[71] J Piekarewicz et al *Phys. Rev. C* **94** 034316 (2016) https://doi.org/10.1103/PhysRevC.94.034316

[72] S R Klein et al *Phys. Rev. C* **60** 014903 (1999) https://doi.org/10.1103/PhysRevC.60.014903

[73] D K Papoulias et al *Front Phys.* (2019) https://doi.org/10.3389/fphy.2019.00191

[74] D G Cerdeno et al *Front. Phys.* **05** 118 (2016) [Erratum: JHEP 09, 048 (2016)]. https://link.springer.com/article/10.1007/JHEP09(2016)048

[75] M Bauer et al *JHEP* (2018) https://doi.org/10.1007/JHEP07(2018)094

[76] G Arcadi et al *Phys. Rev. D* **97** 043009 (2018) https://doi.org/10.1103/PhysRevD.97.043009

[77] M Abdullah et al *Phys. Rev. D* **97** 075035 (2018) https://doi.org/10.1103/PhysRevD.97.075035
[78] Y Farzan *Phys. Lett. B* **803** 135349 (2020) https://www.sciencedirect.com/science/article/pii/S0370269320301532
[79] P Coloma et al *JHEP* **04** 116 (2017) https://doi.org/10.1007/JHEP04(2017)116
[80] M A Corona et al *JHEP* (2022) https://doi.org/10.1007/JHEP05(2022)109
[81] D A Sierra et al *Phys. Rev. D* **06** 141 (2019) https://doi.org/10.1007/JHEP06(2019)141
[82] J Colaresi et al *Phys. Rev. D* **104** 072003 (2021) https://doi.org/10.1103/PhysRevD.104.072003
[83] M Cirelli et al *JCAP* (2013) https://doi.org/10.1088/1475-7516/2013/10/019
[84] O G Miranda et al *JHEP* **05** 130 (2020) https://doi.org/10.1007/JHEP05(2020)130
[85] M Hoferichter et al *Phys. Rev. Lett.* **115** 092301 (2015) https://doi.org/10.1103/PhysRevLett.115.092301
[86] T Aoyama et al *Phys. Rep.* **887** 1 (2020) https://www.sciencedirect.com/science/article/pii/S0370157320302556
[87] G W Bennett et al *Phys. Rev. D* **73** 072003 (2006) https://doi.org/10.1103/PhysRevD.73.072003
[88] B Abi et al *Phys. Rev. Lett.* **126** 141801 (2021) https://doi.org/10.1103/PhysRevLett.126.141801
[89] Y Farzan et al *Front. Phys.* **6** 1 (2018) https://doi.org/10.3389/fphy.2018.00010
[90] Y Du et al *JHEP* **05** 058 (2021) https://doi.org/10.1007/JHEP05(2021)058
[91] C J Stapleford et al *Phys. Rev. D* **94** 093007 (2016) https://doi.org/10.1103/PhysRevD.94.093007
[92] P S Amanik et al *Phys. Rev. D* **75** 083008 (2007) https://doi.org/10.1103/PhysRevD.75.083008
[93] D K Papoulias *Phys. Rev. D* **102** 113004 (2020) https://doi.org/10.1103/PhysRevD.102.113004
[94] J Barranco et al *Int. J. Mod. Phys. A* **27** 1250147 (2012) https://doi.org/10.1142/S0217751X12501473
[95] I Bischer et al *Nuc. Phys. B* **947** 114746 (2019) https://www.sciencedirect.com/science/article/pii/S0550321319302329
[96] D K Papoulias et al *Phys. Lett. B* **747** 454 (2015) https://www.sciencedirect.com/science/article/pii/S037026931500461X
[97] J K Healey et al *Phys. Rev. D* **87** 117301 (2013) https://doi.org/10.1103/PhysRevD.87.117301
[98] M J Penn PhD Thesis (Stanford University, USA) (1995) https://www.slac.stanford.edu/exp/cdms/ScienceResults/Theses/penn.pdf
[99] T Jagemann PhD Thesis (Technical University of Munich, Germany) (2004) https://d-nb.info/973922745/34
[100] D J Griffiths *Introduction to Elementary Particles*, 2nd edn. (Reed College, USA: Wiley) (2008)
[101] A Bonhomme et al *Eur. Phys. J. C* **82** 815 (2022) https://doi.org/10.1140/epjc/s10052-022-10768-1
[102] J I Collar et al *Phys. Rev. D* **103** 122003 (2021) https://doi.org/10.1103/PhysRevD.103.122003
[103] M F Albakry et al *Phys. Rev. D* **105** 122002 (2022) https://doi.org/10.1103/PhysRevD.105.122002
[104] J Lindhard *Kongel. Dan. Vidensk. Selsk., Mat.-Fys. Medd.* **34** (1965) https://www.osti.gov/biblio/4536390
[105] L Singh et al *Phys. Rev. D* **99** 032009 (2019) https://doi.org/10.1103/PhysRevD.99.032009
[106] M K Singh et al *Chinese J. Phys.* **58** 63 (2019) https://doi.org/10.1016/j.cjph.2019.01.006
[107] H B Li et al *Phys. Rev. Lett.* **110** 261301 (2013) https://doi.org/10.1103/PhysRevLett.110.261301
[108] J Liao et al *Phys. Lett. B* **775** 54 (2017) https://www.sciencedirect.com/science/article/pii/S0370269317308584
[109] E Aprile et al *Phys. Rev. Lett.* **126** 091301 (2021) https://doi.org/10.1103/PhysRevLett.126.091301